Title
In Crystallo O2 Cleavage at a Preorganized Triiron Cluster

Journal
Journal of the American Chemical Society, 147(1)

ISSN
0002-7863

Authors
Lee, Heui Beom
Ciolkowski, Nicholas
Field, Mackenzie
et al.

Publication Date
2025-01-08

DOI
10.1021/jacs.4c13492

In Crystallo O_2 Cleavage at a Preorganized Triiron Cluster

Heui Beom Lee†, Nicholas Ciolkowski†, Mackenzie Field, David A. Marchiori, R. David Britt, Michael T. Green, and Jonathan Rittle*

† Authors contributed equally

In Nature, the four-electron reduction of O_2 is catalyzed at preorganized multimetallic active sites. These complex active sites often feature low-coordinate, redox-active metal centers precisely positioned to facilitate rapid O_2 activation processes that obviate the generation of toxic, partially-reduced oxygen species. Very few biomimetic constructs simultaneously recapitulate the complexity and reactivity of these biological cofactors. Herein, we report solid-state O_2 activation at a triiron(II) active site templated by phosphinimide ligands. Insight into the structure of the O_2 reduction intermediates was obtained via *in crystallo* O_2 dosing experiments in conjunction with spectroscopic, structural, magnetic, and computational studies. These data support the *in situ* formation of an $Fe_2^{III}Fe^{IV}$-dioxo intermediate upon O_2 exposure that participates in oxygen atom and hydrogen atom transfer reactivity with exogenous substrates to furnish a stable $Fe^{II}Fe_2^{III}$-oxo species. Combined, these studies provide an extraordinary level of detail into the dynamics of bond forming and breaking processes operative at complex multimetallic active sites.

INTRODUCTION

The activation and reduction of atmospheric small molecules is integral to the function of our global ecology. In particular, reduction of dioxygen is vital for its role in oxidative metabolism and in serving as the primary chemical oxidant for most complex life.[1] To accomplish these processes, organisms have evolved a variety of metalloenzymes which often contain complex multinuclear active sites. For example, many non-heme diiron oxygenases are capable of activating O_2 and directly oxidizing aliphatic C-H bonds.[2, 3] This reactivity has been attributed to a high-valent diiron(IV) dioxo intermediate.[4, 5] Similarly, multicopper oxidases, such as laccase, couple the reduction of dioxygen to the oxidation of organic substrates by employing a tricopper active site as the locus for O_2 activation (Figure 1A).[6, 7] Spectroscopic and computational studies suggest that this site serves to cooperatively bind and reduce dioxygen as a bridging peroxo moiety before subsequent O−O bond cleavage.[8] Analogous mechanisms have been proposed for other multicopper oxidases such as ascorbate oxidase, ceruloplasmin, and others, highlighting the important role that these multi-nuclear active sites play in oxidative metabolism.[9-11]

A longstanding goal of bioinorganic model chemistry lies in the design of functional analogues to elucidate the electronic and geometric structures of reactive, typically unobservable metal-oxo intermediates, to understand these biological systems, and to inform the design of new oxidative catalysts. In this context, a variety of metal complexes competent for O_2 activation at polynuclear sites have been described (Figure 1B-1C). The Tolman group has characterized dicopper peroxo and bis-μ-oxo intermediates derived from the aggregation of a mononuclear Cu^I 1,4,7–triazacyclononane (TACN) complex upon exposure to O_2.[12, 13] Similarly, the Que group has spectroscopically characterized a series of a tris(2-pyridyl)amine (TPA) supported high valent diiron oxo intermediates competent for C-H bond cleavage.[14] These dimeric transition metal complexes represent some of the first synthetic examples of reactive, high-valent metal μ-oxo cores analogous to the proposed intermediates of O_2-reactive diiron enzymes and multicopper oxidases.[15-17] More recently, the Murray group has developed a three-fold symmetric cyclophane cage to support discrete trimetallic active sites.[18] This platform can support a tricopper site capable of *in situ* dioxygen activation and subsequent oxidation of weak C-H bonds.[19] However, characterization of the oxygenated copper intermediates attributed to these transformations was limited due to degradation pathways attributed to oxidation of the cyclophane platform. The transient, reactive nature of many of these oxygenated intermediates underscores the general difficulty in obtaining the desired structural and spectroscopic characterization of these model complexes. In this context, several dinuclear systems have been described, but well-characterized oxygen intermediates of higher nuclearity remain rare.[20-29]

We hypothesized that a multidentate phosphinimide (PN) ligand would be an intriguing platform for addressing these challenges.[30] In the absence of sterically-encumbering phosphorus substituents, PN ligands exhibit a propensity towards bridging multiple metal centers and supporting various metal cluster topologies.[31] However, very few of these systems have been examined within the context of small molecule activation and, in general, their reactivity remains underexplored.[32-36] Herein, we report the synthesis, structural and spectroscopic characterization of a series of trinuclear Fe complexes supported by a multidentate PN architecture that productively react with O_2 (Figure 1D).

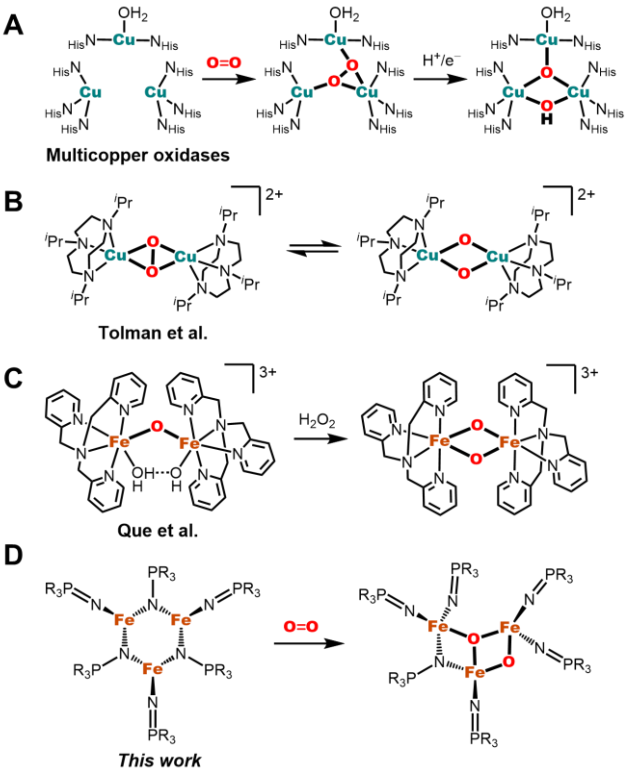

Figure 1. (A) O_2 reduction at the tricopper active site of multicopper oxidases. (B) TACN-supported dicopper peroxo and μ-oxo intermediates. (C) TPA-supported diiron bis μ-oxo intermediate. (D) O_2 reduction at a triiron active site reported in this work.

RESULTS AND DISCUSSION

Synthesis of a Low-coordinate Fe^{II}_3 PN Cluster. Following the observed O_2 reactivity of the Co_3^{II} complex supported by the tris-PN framework, H_3L, we sought to prepare the analogous Fe_3^{II} complex.[37] Treatment of an equivalent of H_3L with 1.5 equivalents of $Fe[N(SiMe_3)_2]_2$ led to the formation of complex **1** and its X-ray crystal structure revealed a $L^{(3-)}_2Fe^{II}_3$ formulation (Figure 2A). While the ligand:metal stoichiometry of **1** is the same as that of the analogous Co_3^{II} complex, the structure of **1** features a pseudo-C_3-symmetric arrangement of Fe centers oriented in a "tri-aza-tri-ferri-cyclohexane" motif (Figure 2B). Each Fe center was found to adopt a trigonal planar geometry ligated by one terminal PN and two bridging PN-derived N-atoms. The terminal Fe–N distances are notably shorter (d_{avg}(Fe-N): 1.857 Å) than those of the bridging Fe–N distances (d_{avg}(Fe-N): 1.963 Å). The long intermetallic distances (d(Fe···Fe): 2.992, 2.9123, and 2.884 Å) reflect a nearly equilateral arrangement of metal ions and marginal metal-metal bonding interactions.[38]

Insight into the electronic structure of **1** was obtained from ^{57}Fe Mössbauer spectroscopy and SQUID magnetometry. Consistent with the C_3 symmetric Fe_3^{II} core of **1**, a single quadrupole doublet with an isomer shift of $\delta = 0.55$ mm/s and a quadrupole splitting of $\Delta E_Q = 0.74$ mm/s was observed at 80 K and zero applied field (Figure S1). The relatively low isomer shift for this triferrous compound can be attributed to substantial covalency within the Fe-PN interactions.[39] For comparison, the spectrum of a trigonal planar, $S = 2$ Fe^{II}-tris-thiolate complex features nearly identical parameters ($\delta = 0.56$ mm/s, $\Delta E_Q = 0.81$ mm/s),[40] and an isomer shift of $\delta = 0.59$ mm/s was observed for a mononuclear, trigonal high spin Fe(II)-PN complex.[30] Hence, the local Fe sites of **1** are presumed to adopt $S = 2$ spin states. Solid-state magnetic studies of **1** revealed a small χT (emu K mol^{-1}) value of 1.5 at 270 K indicative of strong antiferromagnetic coupling between the Fe^{II} sites. This χT value was found to steadily decrease with temperature towards a negligible value at 10 K (Figure 3). This data was effectively simulated with an isotropic spin Hamiltonian that considers an isosceles triangular arrangement of Fe atoms ($H = -2J[S_1 \cdot S_2 + S_1 \cdot S_3] - 2J'[S_2 \cdot S_3]$) with resultant Hamiltonian parameters $g = 2.0$, $J = -100$ cm^{-1}, $J' = -75$ cm^{-1}, $J/J' = 1.33$. Within this framework, a singlet ground state is predicted for $J/J' = 0.7$~1.5 for triangular systems comprised of high spin Fe^{II} centers (Figure S2).[41] Similar antiferromagnetic behavior has been observed in other trigonal Fe^{II}_3 complexes that feature bridging alkoxides/acetates[42] or hydride ligands[43]. However, the comparatively smaller exchange coupling constants ($J = -1$ to -14 cm^{-1}) inferred from these systems manifest low-lying, paramagnetic excited states that are appreciably populated at low temperature. In contrast, the diamagnetic behavior observed for **1** below 20 K results from the large J values that raise the energy of paramagnetic excited states.[44] Comparable exchange coupling constants were determined for the analogous L_2Co_3 system and collectively suggest that bridging phosphinimide groups provide an efficient pathway for magnetic superexchange interactions.[37, 45]

***In Crystallo* O_2 Activation Studies.** The cyclic- and square wave voltammograms of **1** in 0.2 M [^{n}Bu$_4$N][PF$_6$] electrolyte in THF revealed a reversible oxidation event at $E = -1.1$ V vs. Fc/Fc$^+$, and two additional, quasi-reversible oxidation processes at $E = -0.55$ V and $E = -0.1$ V (Figure S3-S4). Presumably, these oxidation processes generate cationic L_2Fe_3 species bearing one or more high-spin Fe^{III} ions (**1**$^{n+}$, $n = 1, 2, 3$). Attempts to prepare **1**$^{n+}$ derivatives via chemical oxidation unfortunately resulted in the formation of intractable mixtures of species. Nonetheless, these electrochemical data indicate that **1** could mediate multi-electron reduction processes. Indeed, the solid-state architecture of **1** contains a substantial cleft near the centroid of the N(4)-N(5)-N(6) plane (Figure 2B) that could support the binding of small molecules. In addition, the loosely-packed crystal lattice of **1** is comprised of low occupancy solvent channels that may permit direct solid-gas experiments (Figure S5).

In anticipation that these low-coordinate iron sites were poised for cooperative small molecule activation, the reactivity of **1** with O_2 was explored. An O_2 titration with complex **1** (2-MeTHF, -30 °C) indicated that 1 molar equiv O_2 was consumed (Figure S6) alongside the formation of a broad absorbance feature centered at ~380 nm. The resultant species was stable at these temperatures to additional O_2, but the pronounced insolubility of **1** and its derivatives in common organic solvents precluded additional solution-phase characterization. Fortunately, the crystallinity of single crystals of **1** was not diminished following their exposure to dry O_2, despite visible darkening of the solid material. X-ray diffraction studies performed after 24 hours of O_2 exposure revealed the formation of a new triiron complex (**2**) harboring a bridging oxo (μ^3-O) ligand. Complex **2** was also independently prepared via treatment of a slurry of **1** in pyridine with one equivalent of iodosylbenzene (Figure 2A). The Fe centers of **2** adopt local geometries that are intermediate between tetrahedral and trigonal monopyramidal ($\tau(4)_{avg}$: 0.61)[46] and exhibit Fe–(μ^3-O) distances of 1.844(2), 1.928(2), and 1.941(2) Å (Figure 2B) which are comparable to

the numerous molecular complexes and MOFs featuring triangular $Fe^{II}Fe_2^{III}(\mu^3\text{-}O)$ cores.[47, 48] The intermetallic distances in **2** (d(Fe···Fe): 2.7315(7), 2.6930(7), and 2.6752(6) Å) are contracted by ~0.2 Å relative to **1** and indicate that the ligand architecture and crystalline lattice readily support structurally-dynamic clusters in the solid state.

The 80 K ^{57}Fe Mössbauer spectrum of polycrystalline **2** features two resolved quadrupole doublets in a 2:1 ratio (Figure 2C) that intimate a mixed-valent $Fe^{II}Fe^{III}_2$ formulation.[49] On the basis of the pseudo-C_3 symmetry of the Fe_3O core in **2**, the narrower doublet was fit to two quadrupole sub-doublets with similar isomer shifts, and correspond to two Fe^{III} centers. At 200 K, the high velocity feature associated with the Fe^{II} quadrupole doublet exhibited weaker intensity relative to that observed at 80 K. Similar temperature-dependent behavior has been observed for other complexes featuring $Fe^{II}Fe^{III}_2O$ cores,[47, 50] and has been attributed to valence-delocalized states at higher temperatures (Figure S7). However, the magnetochemistry of **2** (*vide infra*) indicate that Mössbauer studies at much lower temperatures would be required to confirm these hypotheses.

For complex **2**, the χT value of 6.0 at 270 K was found to decrease slowly with temperature down to 20 K (Figure 3). Further cooling resulted in a rapid decrease to assume a χT value of 3.2 at 4 K, consistent with the expected value of 3.0 for an $S_{TOT} = 2$ ground state. The temperature dependence of χT within the low temperature regime implicates the presence of a low-lying $S_{TOT} = 3$ excited state. The magnetometry data was effectively simulated by assuming two equivalent Fe^{II}-Fe^{III} exchange interactions (J) and a second Fe^{III}-Fe^{III} exchange interaction (J'). The simulated line in Figure 3 employs the following isotropic spin Hamiltonian parameters: $g = 2.05$, $J = +60 \pm 5$ cm^{-1}, $J' = -120 \pm 10$ cm^{-1}. Within this framework, the $S_{TOT} = 2$ ground state is predicted for $J/J' = -0.5$~0, consistent with the experimental value of $J/J' = -0.49$ (Figure S8). The *ferromagnetic* Fe^{II}-Fe^{III} interaction is noteworthy and distinct from that found for canonical Fe_3O clusters.[51, 52] The $[Fe_3O]^{6+}$ cores in these systems are planar, which manifest antiferromagnetic superexchange interactions via the trigonal planar bridging O^{2-} ligand. In contrast, the oxo ligand of **2** is strongly pyramidalized, and the acute ∠Fe-O-Fe angles of 87.5°~92.8° found in **2** are expected to favor ferromagnetic interactions.[53] Moreover, the intermetallic distances in **2** (*vide supra*) are much shorter than those found in planar $[Fe_3O]^{6+}$ clusters (~3.3 Å), increasing the plausibility of direct metal-metal bonding,[54] that often result in ferromagnetic double exchange interactions within valence delocalized systems.[55]

The O_2-mediated formation of the $Fe_3(O)$ **2** within single crystals of **1** prompted us to search for conditions that would allow the observation of earlier intermediates containing both O_2-derived O-atoms. Small crystals of **1** were briefly exposed (~30 minutes) to dry O_2 and examined using synchrotron radiation-based X-ray diffraction experiments. Gratifyingly, the obtained diffraction data revealed two distinct components each representing ~50% of the sample. One of the components was readily assigned as **2** on the basis of a similar $[Fe_3O]$ core structure (Table S1). The other component contains a $L_2Fe_3(O)(OH)$ cluster (**3**, Figure 4A). There are three notable differences between the two crystallographic components. First, the $Fe_3(\mu^3\text{-}O)$ core of **3** is appreciably more distorted than that of **2**, with one long intermetallic distance (d(Fe(1)···Fe(2)): 3.380(2) Å) that gives rise to a unique, weaker Fe-(μ^3-O) interaction (d(Fe(1)-O(1): 2.052(4) Å) than that of the adjacent interactions

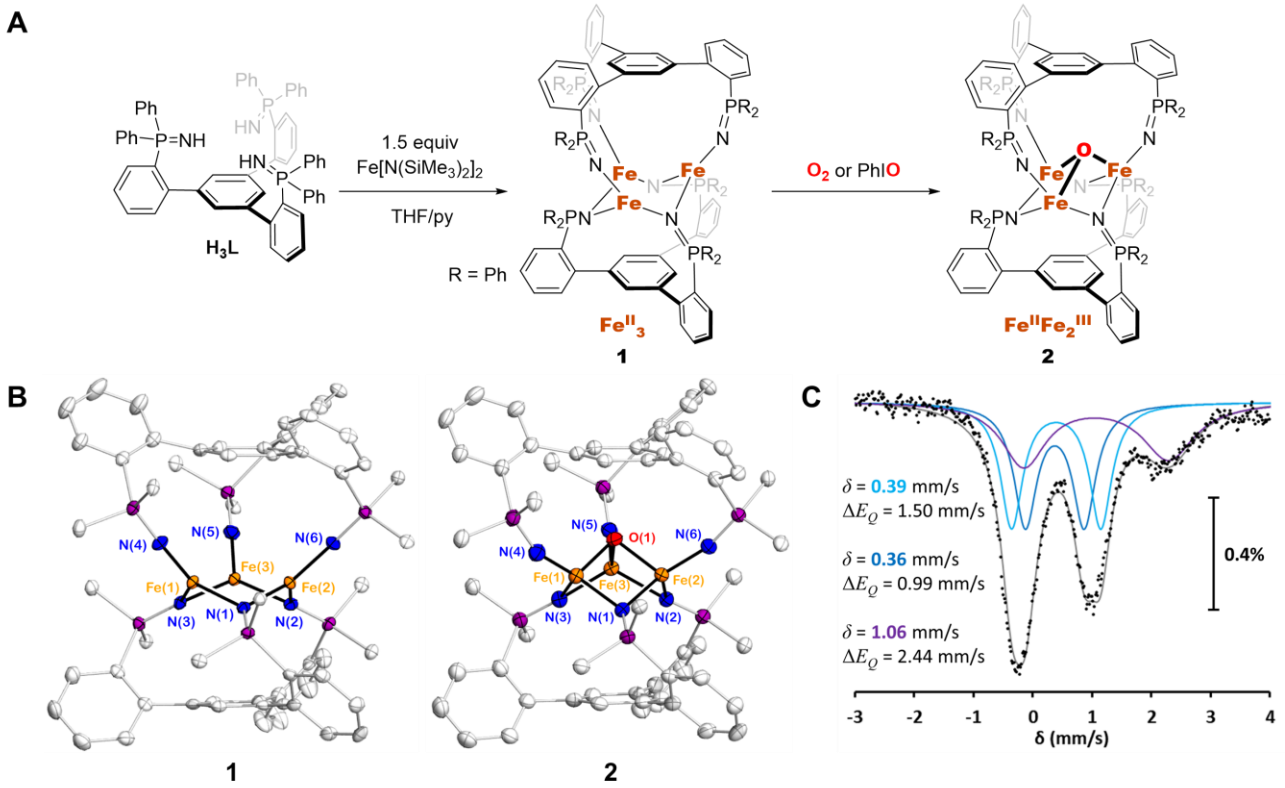

Figure 2. (A) Synthesis of the triiron complexes **1** and **2** from the trisphosphinimine H_3L. (B) Truncated crystal structure of **1** (left) and **2** (right). (C) Zero field Mössbauer spectrum of **2** collected at 80 K and corresponding fit of the data using three quadrupole doublets of equal areas.

(Table S2). Second, a bridging PN-derived N-atom was found to have dissociated from Fe(1) to allow coordination of a second oxygen atom, O(2) (Figure 4A). The short Fe(1)–O(2) distance of 1.869(7) Å is most consistent with a terminal iron-hydroxo assignment.[56, 57] This hydroxo ligand lies in close proximity to the dechelated phosphinimide nitrogen (d(N(1) ···O(2)): 2.86(1) Å) and an adventitious water molecule (d(O(2)–O(3)): 2.69(1) Å) intimating the presence of a strong hydrogen bonding interaction between these moieties. Finally, the aryl substituents adjacent to the hydroxo ligand adopt distinct conformations between **2** and **3** to accommodate its steric influence (Figure S9).

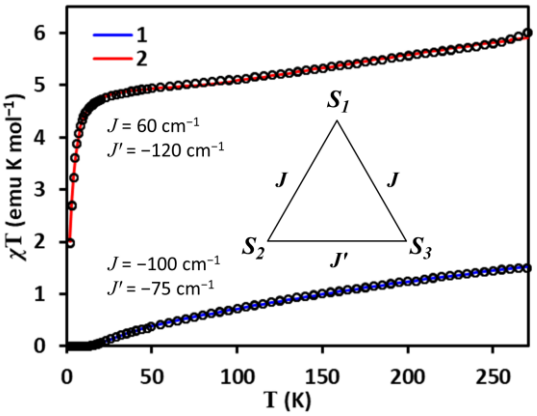

Figure 3. χT vs T plot of the magnetic susceptibility data of **1** and **2** and corresponding fit using an isosceles triangular arrangement of Fe atoms. See text for spin Hamiltonian.

The *in crystallo* formation of **3** is undoubtedly complex, but we hypothesize that it is a metastable intermediate derived from O_2 activation by **1** and its $(Fe^{III})_3$ formulation is corroborated by Electron Paramagnetic Resonance (EPR) spectroscopy on solution-phase samples (*vide infra).* The crystallographic snapshots suggest that following O_2 activation by **1**, sequential hydrogen atom transfer processes generate $Fe_3(O)(OH)$ **3** followed by the formation of $Fe_3(O)$ **2** and the loss of water (Figure 4B). While intermediates preceding the formation of **3** cannot be observed crystallographically, they likely include a a triiron-dioxo (^{O}**4,** $Fe^{IV}Fe^{III}_2(O)_2$) species and/or a triiron-peroxo species (^{P}**4,** $Fe^{II}Fe^{III}_2(O_2)$) (Figure 5). Taken together, the available crystallographic data supports the notion that cooperative O_2 activation occurs at the Fe_3^{II} core of **1** in the solid state.

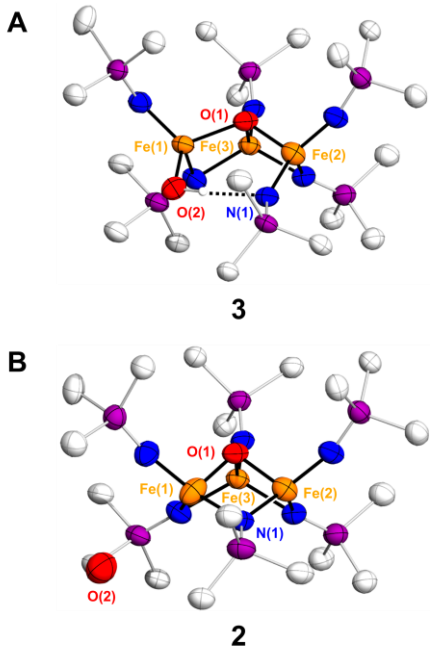

Figure 4. Truncated crystal structures of the two components observed upon *in crystallo* oxygenation of **1**, leading to complexes (A) **3** and (B) **2**.

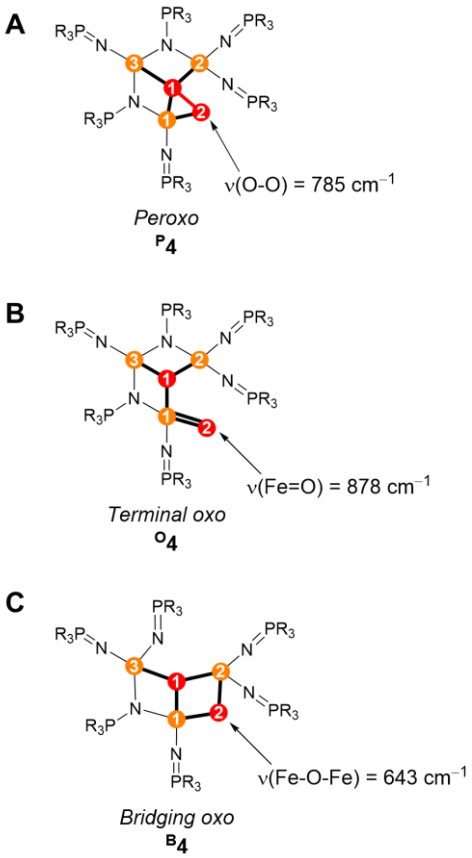

Figure 5. Candidate molecular structures of **4** and corresponding calculated vibrational frequencies. (A) Peroxo ^{P}**4**. (B) Terminal oxo ^{O}**4**. (C) Bridging oxo ^{B}**4**. Orange and red spheres denote Fe and O atoms, respectively.

Spectroscopic Characterization of an Early Intermediate in the Solid State O_2 Activation Process. The multistep conversion of **1** to **3** and **2** requires O_2 and H^+/e^- equivalents stemming from unknown origin within the crystal lattice. In principle, the C-H bonds present within the ligand frameworks could serve as the hydrogen atom source but these groups are not detectably perturbed in the structures of oxygenated complexes. Accordingly, we hypothesize that the requisite H^+/e^- equivalents needed to successively transform the putative ^{P}**4** or ^{O}**4** intermediate(s) to **3** and **2** derive from the co-crystallized Et_2O solvent that contains activated C-H bonds. To explore this hypothesis and ascertain the identity of early intermediates in the O_2 activation process by **1,** we sought to generate solid-state samples of the direct product of O_2 addition to **1**. Crystalline samples of **1** were ground to a fine powder and exhaustively evacuated to remove co-crystallized solvents (Et_2O and pyridine). Subsequent oxygenation (18 hours) with 1 atm dry O_2 resulted in a visible darkening of the solid material alongside quantitative conversion of the Infrared (IR) and ^{57}Fe Mossbauer spectral features of **1**.

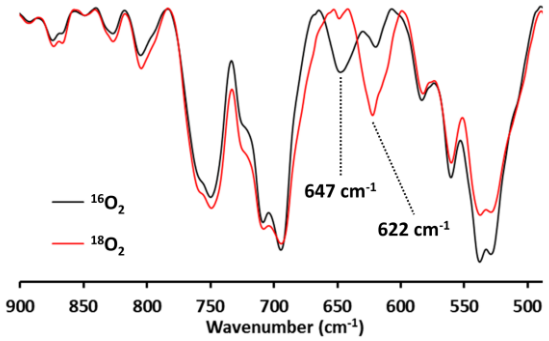

Figure 6. Fingerprint region of the FT-IR spectrum of **4** obtained from $^{16}O_2$ (black trace) and $^{18}O_2$ (red trace).

Monitoring this oxygenation process by FTIR spectroscopy revealed the loss of a prominent peak in **1** at 1252 cm^{-1}, and growth of a new peak at 1200 cm^{-1} (Figure S10). These features are ascribed to ν(P=N) stretching frequencies stemming specifically from the terminally-bonded PN ligands and the lower energy in the product (**4**) is consistent with a higher total Fe oxidation state.[58] A similar feature (1202 cm^{-1}), albeit with diminished intensity, is also observed in **2**. Exposure of **1** to natural abundance or ^{18}O-labelled O_2 was found to furnish a single isotopically-sensitive IR band at 647 cm^{-1} and 622 cm^{-1}, respectively (Figure 6), confirming the incorporation of O_2 in **4**. The observed spectral shift is consistent with a $^{16}O/^{18}O$ reduced mass consideration but the magnitude of the vibrational frequency substantially constrains the plausibility of candidate oxygenated iron (Fe_xO_y) fragments present in **4**. For example, terminal iron-oxo and diiron-peroxo units are unlikely to be present in **4** as these chemical units typically exhibit vibrational features in the range of 800~900 cm^{-1} that correspond to the ν(Fe=O) and ν(O-O) vibrational modes, respectively.[59] In principle, the energy of this feature is consistent with a terminal Fe-OH unit[60] but the absence of a corresponding ν(O-H) features rules out this possibility (Figure S10). Hence, we favor the presence of either a diiron-peroxo or diiron-dioxo fragment interacting with an additional Lewis acidic center (Fe or P) to rationalize the low energy vibrational mode of **4**.

The ^{57}Fe Mössbauer spectra obtained following the conversion of **1** to **4** (Figure 7A) reveal quantitative consumption of **1** after 18 hours of exposure to dry O_2. While the higher velocity side of the spectrum of **4** is an overlapping broad signal, the lower velocity side presents two inflection points at −0.3 mm/s and 0 mm/s, suggesting the presence of three distinct Fe centers. Several satisfactory fits were obtained (Figure S11); however, we favor the simulation (Figure 7B) in which the parameters for two of the sub-doublets closely resemble those assigned to the Fe^{III} centers in **2**. In this simulation, the remaining quadrupole doublet exhibits a comparably low isomer shift of $\delta = 0.23$ mm/s implicating either a high-spin Fe^{IV} center or a low-spin Fe^{II} center in **4**.[61-63] Owing to their strongly π-basic nature, PN ligands present a weak ligand field,[37] and their ligation to low-coordinate FeO_x fragments are expected to culminate in local high spin configurations, as found for **1** and **2**. While low-spin Fe-PN complexes have been prepared, these complexes additionally contain two or more strong-field phosphine or carbene co-ligands.[58, 64] Accordingly, our preferred interpretation of the available ^{57}Fe Mössbauer data on **4** implicate the presence of two high-spin Fe^{III} ions and one high-spin Fe^{IV} ion.

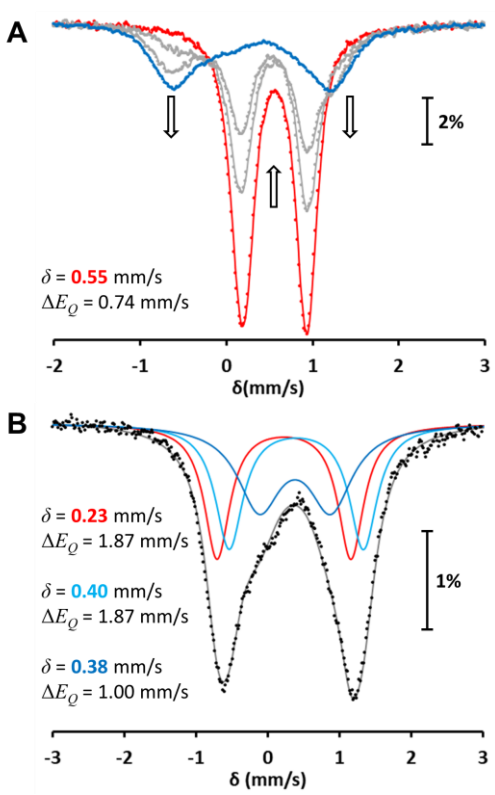

Figure 7. Zero field Mössbauer spectra collected at 80 K. (A) Conversion of complex **1** (red points) to **4** (blue points) upon oxygenation in the solid state. Lines are for guide only. (B) Fit of the data of **4** using three quadrupole doublets of equal areas.

Computational Investigations Implicate in situ formation of a triiron-dioxo Species. Computational investigations were pursued to correlate the spectroscopic features of **4** with candidate molecular structures. Geometry optimizations were carried out using the TPSSh functional and 6-31G(d) basis set for all atoms. We considered $L_2Fe_3O_2$ formulations of **4** that contained a terminal oxo group (^{O}**4**), a bridging oxo group (^{B}**4**), or an intact O-O bond of the dioxygen fragment (^{P}**4**) (Figure 5). For the input geometry of ^{P}**4**, the ∠O(2)-Fe(1)-O(1) angle of **3** was reduced in order to introduce O-O bonding interactions (d(O-O): 1.45 Å) expected for a bridging peroxo formulation (Figure 5A). The input geometry of ^{O}**4** was prepared via the simple removal of hydroxide H-atom from **3** and a shortening of the Fe(1)-O(1) bond distance to 1.65 Å (Figure 5B). In all cases, the gas-phase geometries were optimized in their S_{TOT} = 7 spin states. These spin states were selected as the only assumption is the presence of two high-spin Fe^{III} ions and a high-spin Fe^{IV} ion in ^{O}**4** or high-spin Fe^{II} ion in ^{P}**4**, and is agnostic to the specific locations of the unique ions. Lower total spin ground states resulting from antiferromagnetic interactions are likely present in **4**. However, owing to the divergent spin-coupling behavior observed in **1** and **2**, the absence of structural data on **4**, and the large size of the complexes (227 atoms) we were hesitant to optimize the various broken symmetry wavefunctions for each of the candidate geometries. Thus, these computational studies are necessarily deficient in their ability to understand the cluster spin energetics and metal-metal bonding interactions of **4**. Nonetheless, their value lies in understanding the nature of the hallmark $^{18/16}$O-sensitive IR vibration of **4.**

The optimized geometry found for ^{P}**4** indicate the presence of an unsymmetrically coordinated peroxo ligand (O_2^{2-}) positioned between a T-shaped arrangement of three, four-coordinate iron centers (d(O-O): 1.516 Å, Figure 5A). To accommodate the central peroxo ligand, only two PN ligands were found to adopt μ^2-coordination modes and this results in one long intermetallic distance (d(Fe(1)···Fe(2)): 3.902 Å). The peroxo ligand was found to preferentially interact with Fe(1) in a side-on bridging manner and via weaker monodentate interactions with Fe(2) and Fe(3) (d(Fe(2/3)-O(1): 1.987 and 2.193 Å, respectively). The difference of the predicted FTIR spectra for ^{P}**4** and ^{18}**O-**^{P}**4** (Figure S12) indicate that this species should exhibit a feature at 785 cm^{-1} that downshifts to ~740 cm^{-1} upon ^{18}O-labelling and correspond to the ν(O–O) stretching mode.[65, 66] Since such a feature was not observed in the experimental FTIR spectrum of **4** (Figure 6), we ruled out this candidate structure.

The optimized structure of ^{O}**4** reveals a terminal ferryl (Fe=O) unit incorporated within a Fe_3-(μ^3-O) core (Figure 5B). As found for **3**, this iron center is pseudotetrahedral and is coordinated to only one bridging PN group. Here, the Mulliken spin density found for Fe(1) (3.3 unpaired electrons) is significantly lower than those of the other Fe sites (~4.1 unpaired electrons) allowing assignment of the former as a localized Fe^{IV} site. These spin densities are, of course, diminished relative to isolated Fe(III) and Fe(IV) ions owing to the high covalency associated with the Fe-O and Fe-PN bonds.[37] The short iron oxygen bond (d(Fe(1)-O(2)): 1.642 Å) is accompanied by the appearance of a ν(Fe=O) mode at 878 cm^{-1} in the predicted FTIR spectrum (Figure S13). Obviously, this value is incongruent

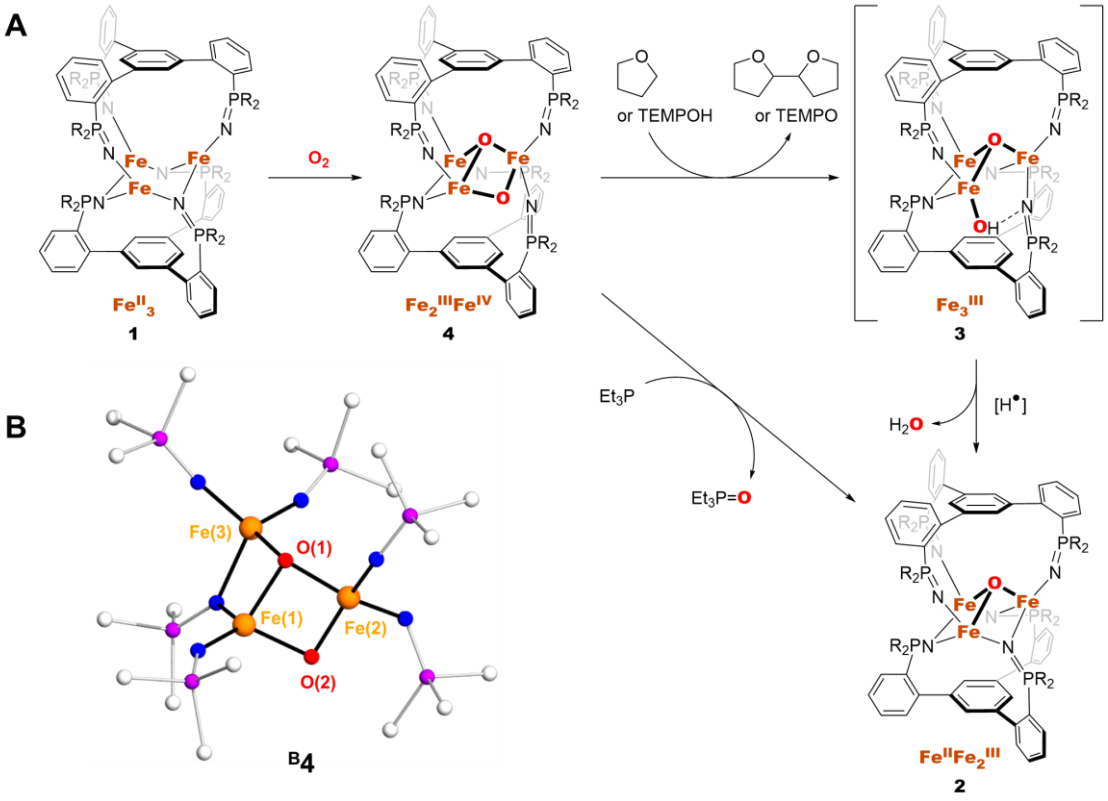

Figure 8. (A) Solid state oxygenation of **1** leads to the formation of **4**. Subsequent hydrogen and oxygen atom transfer reactivity leading to the formation of **2** via the intermediate **3**. (B) Truncated core of the DFT-optimized geometry of ^{B}**4**, featuring a high-valent $Fe_3(\mu^3\text{-O})(\mu^2\text{-O})$ core.

with the experimental FTIR data obtained on **4**. Nonetheless, the Mossbauer data on **4** implicates the presence of a single Fe^{IV} ion, and the comparative free energies of ^{O}**4** from ^{P}**4** suggests that O−O bond cleavage in this system is exergonic by ~50 kcal/mol. This suggests that an alternative structural isomer of ^{O}**4** with a broken O−O bond must exist.

The optimized structure containing a $Fe_3(\mu^3\text{-O})(\mu^2\text{-O})$ unit (^{B}**4**) was deemed as the most likely structure for **4**. This structure (Figure 5C) features three pseudotetrahedral Fe sites that accommodate the additional bridging oxo by forcing the conversion of two bridging phosphinimide ligands to adopt terminal binding modes. This structural evolution is supported by the experimental FTIR data (Figure S10) on **4** which contains comparatively stronger ν(P=N) absorption features expected for terminally bonded configurations. Despite this geometric deformation, the Gibbs free energy of ^{B}**4** was found to lie ~6 kcal/mol lower in energy than that of ^{O}**4** (Table S6) and its predicted FTIR spectrum (Figure S14) reveals an absorption feature at 643 cm^{-1} that shifts to 621 cm^{-1} upon $^{18}O_2$ substitution. This feature is in excellent agreement with the experimental values (647 and 622 cm^{-1}) and corresponds to an Fe-O-Fe breathing mode (Figure S15) comparable to those found in diiron(IV)-bis(μ^2-O) complexes which exhibit similar features in the range of 600~700 cm^{-1}.[67] For ^{B}**4**, the Mulliken spin density found for Fe(2) (3.4 unpaired electrons) is significantly lower than those of the other Fe sites (~4.1 unpaired electrons) allowing assignment of the former as a localized Fe^{IV} site. Additionally, the calculated distance of d(Fe(2)-O(2)): 1.777 Å compared to that of d(Fe(1)-O(2)): 1.904 Å further supports this assignment (Table S7). Collectively, these computational investigations corroborate the available spectroscopic data obtained on **4** and rationalize the high reactivity observed for this O_2-derived triiron species.

Reactivity of the Triiron-dioxo Intermediate. The high-valent nature predicted for **4** implicates its involvement in the putative hydrogen atom abstraction processes observed *in crystallo* that furnish intermediates **3** and **2**. We hence investigated the formation of paramagnetic species upon stoichiometric hydrogen atom addition to **4** with Electron Paramagnetic Resonance (EPR) spectroscopy. A slurry of solid **4** in a 2-MeTHF solution containing 1 equiv of TEMPOH was frozen after 5 minutes of rapid stirring at room temperature. X-band EPR spectra (Figure S16-S17) of these samples revealed intense signals at low fields ascribable to an S_{TOT} = 5/2 species. A feature at g = 8.9 can be assigned to the $|\pm1/2\rangle$ Kramers doublet of an S_{TOT} = 5/2 species with intermediate rhombicity E/D = 0.17. Additional transitions at g = 5.2, 3.5, and 3.1 can be assigned to the $|\pm3/2\rangle$ Kramers doublet of the same spin state and rhombicity, indicating that all four transitions observed in the presence of TEMPOH likely arise from a single species, assigned as **3**. The S_{TOT} = 5/2 spin state of **3** is consistent with the Fe_3^{III} formulation, and can be further understood in the context of its crystal structure. On the basis of a distinctly elongated Fe(1)−Fe(2) distance in **3**, a small J_{12} coupling is expected. For such a case, the S_{TOT} = 5/2 state is expected to be the ground state; for high-spin Fe_3^{III} complexes featuring a linear or a T-shaped arrangement of Fe centers, an S_{TOT} = 5/2 ground state is observed.[68, 69] In contrast, an S_{TOT} = 1/2 ground state is observed for Fe_3^{III} complexes featuring a more symmetric core in which all three J values are similar to each other.[69, 70]

Compound **4** was additionally found to react with prototypical oxygen atom acceptors and hydrogen atom donors (Figure 8A). Under N_2, treatment of a suspension of **4** in pentane with an equivalent of Et_3P resulted in the formation of 0.76 equivalents of Et_3PO (Figure S18) over 10 days. Similarly, treatment with excess TEMPOH led to the formation of 2.0 equivalents of TEMPO (Figure S19) over 3 days. The sluggish nature of these OAT and HAT reactions are likely a consequence of the highly-insoluble nature of **4** combined with the steric impact of the twelve phenyl substituents that surround the Fe_3 site. In the reaction with TEMPOH, the $Fe_3(\mu^3\text{-O})$ species **2** was identified as the dominant inorganic product (Figure S20). This reaction can be viewed as a model for the crystallographically observed decay of **4** to **2** via **3** by hydrogen atom transfer (Figure 4). Moreover, following overnight exposure of **4** to THF under an inert atmosphere, both isomers of 2,2'-octahydrobifuran (diTHF, Figure S21) are observed by GC-MS. This organic product is not observed from similarly prepared reaction mixtures that instead employ **1** or **2**. These observations are consistent with α-C-H bond abstraction of THF by **4** to furnish **3** and a 2-tetrahydrofuranyl radical that, in turn, can dimerize to form diTHF in the absence of additional equivalents of O_2.[56] Taken together, the reactivity of **4** is comparable to other synthetic high-valent, multinuclear iron-and copper-oxo complexes which are often prepared with oxidants other than O_2.[71-73]

CONCLUSIONS

Our data demonstrates that a triferrous cluster featuring low-coordinate metal sites reacts with O_2 both *in crystallo* and in powdered form to afford products consistent with the complete cleavage of O_2. The resultant $[Fe_3(\mu^3\text{-O})(\mu^2\text{-O})]^{6+}$ species (Figure 8B) derived from this reaction was shown to engage in both oxygen atom transfer and hydrogen atom transfer reactivity. The structures of the inorganic intermediates and products of these reactions were resolved by *in situ* O_2 dosing experiments performed on single crystals and EPR studies of an unusual triiron oxo-hydroxo species. Collectively, these studies highlight phosphinimide ligands as electron donating, oxidatively-robust, and coordinatively flexible ligands that allow for the creation of reactive multimetallic fragments whose ability to mediate facile small molecule activation processes is comparable to those found in natural enzymes. We anticipate that these systems are likely to engage other small, gaseous molecules (e.g., NO and CO) and are presently investigating this possibility.

ASSOCIATED CONTENT

Supporting Information

The Supporting Information is available free of charge at https://pubs.acs.org/doi/10.1021/jacs.XXXXXXX.

Experimental procedures, crystal structures, reactivity and characterization data, theoretical studies, Figures S1−S21, Tables S1−S6.

AUTHOR INFORMATION

Corresponding Author

Jonathan Rittle − Department of Chemistry, University of California Berkeley, Berkeley, California 94720, United States; orcid.org/0000-0001-6241-6253; Email: rittle@berkeley.edu

Authors

Heui Beom Lee − Department of Chemistry, University of California Berkeley, Berkeley, California 94720, United States; orcid.org/0000-0002-9550-2649

Nicholas Ciolkowski − Department of Chemistry, University of California Berkeley, Berkeley, California 94720, United States; https://orcid.org/0000-0002-7769-3912

Mackenzie Field − Department of Chemistry and Department of Molecular Biology and Biochemistry, University of California, Irvine, California 92697, United States

David A. Marchiori − Department of Chemistry, University of California Davis, Davis, California 95616, United States; orcid.org/0000-0001-9738-3674

R. David Britt − Department of Chemistry, University of California Davis, Davis, California 95616, United States; orcid.org/0000-0003-0889-8436

Michael T. Green − Department of Chemistry and Department of Molecular Biology and Biochemistry, University of California, Irvine, California 92697, United States; orcid.org/0000-0001-8658-8420

Notes

The authors declare no competing financial interest.

ACKNOWLEDGMENTS

This research was supported by the University of California Berkeley. We thank Dr. Nicholas Settineri for assistance with XRD experiments. A portion of the XRD studies was performed at beamline 9-2 of the Stanford Synchrotron Radiation Lightsource, SLAC National Accelerator Laboratory, supported by the U.S. Department of Energy, Office of Science, Office of Basic Energy Sciences under Contract No. DE-AC02-76SF00515. We thank Prof. Kwabena Bediako for access to a SQUID magnetometer and Zhizhi Kong for assistance. M.J.F. was supported by a National Sciences and Engineering Research Council of Canada (NSERC) Postgraduate Scholarship.

References

(1) Gray, H. B.; Winkler, J. R. Living with Oxygen. *Acc. Chem. Res.* **2018**, *51* (8), 1850-1857 DOI: 10.1021/acs.accounts.8b00245.

(2) Baik, M.-H.; Newcomb, M.; Friesner, R. A.; Lippard, S. J. Mechanistic Studies on the Hydroxylation of Methane by Methane Monooxygenase. *Chem. Rev.* **2003**, *103* (6), 2385-2420 DOI: 10.1021/cr950244f.

(3) Jasniewski, A. J.; Que, L. Dioxygen Activation by Nonheme Diiron Enzymes: Diverse Dioxygen Adducts, High-Valent Intermediates, and Related Model Complexes. *Chem. Rev.* **2018**, *118* (5), 2554-2592 DOI: 10.1021/acs.chemrev.7b00457.

(4) Castillo, R. G.; Banerjee, R.; Allpress, C. J.; Rohde, G. T.; Bill, E.; Que, L.; Lipscomb, J. D.; DeBeer, S. High-Energy-Resolution Fluorescence-Detected X-ray Absorption of the Q Intermediate of Soluble Methane Monooxygenase. *J. Am. Chem. Soc.* **2017**, *139* (49), 18024-18033 DOI: 10.1021/jacs.7b09560.

(5) Liu, K. E.; Valentine, A. M.; Salifoglou, A.; Lippard, S. J.; Wang, D.; Huynh, B. H.; Edmondson, D. E. Kinetic and Spectroscopic Characterization of Intermediates and Component Interactions in Reactions of Methane Monooxygenase from Methylococcus capsulatus (Bath). *J. Am. Chem. Soc.* **1995**, *117* (41), 10174-10185 DOI: 10.1021/ja00146a002.

(6) Jones, S. M.; Solomon, E. I. Electron transfer and reaction mechanism of laccases. *Cell. Mol. Life Sci.* **2015**, *72* (5), 869-883 DOI: 10.1007/s00018-014-1826-6.

(7) Solomon, E. I.; Heppner, D. E.; Johnston, E. M.; Ginsbach, J. W.; Cirera, J.; Qayyum, M.; Kieber-Emmons, M. T.; Kjaergaard, C. H.; Hadt, R. G.; Tian, L. Copper active sites in biology. *Chem. Rev.* **2014**, *114* (7), 3659-3853 DOI: 10.1021/cr400327t.

(8) Yoon, J.; Solomon, E. I. Electronic structure of the peroxy intermediate and its correlation to the native intermediate in the multicopper oxidases: Insights into the reductive cleavage of the O-O bond. *J. Am. Chem. Soc.* **2007**, *129* (43), 13127-13136 DOI: 10.1021/ja073947a.

(9) Messerschmidt, A.; Huber, R. The blue oxidases, ascorbate oxidase, laccase and ceruloplasmin Modelling and structural relationships. *Eur. J. Biochem.* **1990**, *187* (2), 341-352 DOI: 10.1111/j.1432-1033.1990.tb15311.x.

(10) Messerschmidt, A.; Rossi, A.; Ladenstein, R.; Huber, R.; Bolognesi, M.; Gatti, G.; Marchesini, A.; Petruzzelli, R.; Finazzi-Agró, A. X-ray crystal structure of the blue oxidase ascorbate oxidase from Zucchini. Analysis of the polypeptide fold and a model of the copper sites and ligands. *J. Mol. Biol.* **1989**, *206* (3), 513-529 DOI: 10.1016/0022-2836(89)90498-1.

(11) Solomon, E. I.; Sundaram, U. M.; Machonkin, T. E. Multicopper Oxidases and Oxygenases. *Chem. Rev.* **1996**, *96* (7), 2563-2606 DOI: 10.1021/cr950046o.

(12) Mahapatra, S.; Halfen, J. A.; Wilkinson, E. C.; Pan, G.; Wang, X.; Young, V. G.; Cramer, C. J.; Que, L.; Tolman, W. B. Structural, spectroscopic, and theoretical characterization of bis(μ-oxo)dicopper complexes, novel intermediates in copper-mediated dioxygen activation. *J. Am. Chem. Soc.* **1996**, *118* (46), 11555-11574 DOI: 10.1021/ja962305c.

(13) Halfen, J. A.; Mahapatra, S.; Wilkinson, E. C.; Kaderli, S.; Young, V. G.; Que, L.; Zuberbühler, A. D.; Tolman, W. B. Reversible Cleavage and Formation of the Dioxygen O-O Bond Within a Dicopper Complex. *Science* **1996**, *271* (5254), 1397-1400 DOI: 10.1126/science.271.5254.1397.

(14) Dong, Y.; Fujii, H.; Hendrich, M. P.; Leising, R. A.; Pan, G.; Randall, C. R.; Wilkinson, E. C.; Zang, Y.; Que, L. A High-Valent Nonheme Iron Intermediate. Structure and Properties of $[Fe_2(\mu\text{-}O)_2(5\text{-}Me\text{-}TPA)_2](ClO_4)_3$. *J. Am. Chem. Soc.* **1995**, *117* (10), 2778-2792 DOI: 10.1021/ja00115a013.

(15) Mirica, L. M.; Ottenwaelder, X.; Stack, T. D. P. Structure and Spectroscopy of Copper−Dioxygen Complexes. *Chem. Rev.* **2004**, *104* (2), 1013-1046 DOI: 10.1021/cr020632z.

(16) Lewis, E. A.; Tolman, W. B. Reactivity of Dioxygen−Copper Systems. *Chem. Rev.* **2004**, *104* (2), 1047-1076 DOI: 10.1021/cr020633r.

(17) Merkx, M.; Kopp, D. A.; Sazinsky, M. H.; Blazyk, J. L.; Müller, J.; Lippard, S. J. Dioxygen Activation and Methane Hydroxylation by Soluble Methane Monooxygenase: A Tale of Two Irons and Three Proteins. *Angew. Chem. Int. Ed.* **2001**, *40* (15), 2782-2807 DOI: 10.1002/1521-3773(20010803)40:15<2782::AID-ANIE2782>3.0.CO;2-P.

(18) Guillet, G. L.; Sloane, F. T.; Ermert, D. M.; Calkins, M. W.; Peprah, M. K.; Knowles, E. S.; Cižmár, E.; Abboud, K. A.; Meiselb, M. W.; Murray, L. J. Preorganized assembly of three iron(II) or manganese(II) β-diketiminate complexes using a cyclophane ligand. *Chem. Commun.* **2013**, *49* (59), 6635-6637 DOI: 10.1039/c3cc43395a.

(19) Cook, B. J.; Di Francesco, G. N.; Kieber-Emmons, M. T.; Murray, L. J. A Tricopper(I) Complex Competent for O Atom Transfer, C-H Bond Activation, and Multiple O_2 Activation Steps. *Inorg. Chem.* **2018**, *57* (18), 11361-11368 DOI: 10.1021/acs.inorgchem.8b00921.

(20) Zheng, H.; Zang, Y.; Dong, Y.; Young, V. G.; Que, L. Complexes with $Fe^{III2}(\mu\text{-}O)(\mu\text{-}OH)$, $Fe^{III2}(\mu\text{-}O)_2$, and $[Fe^{III3}(\mu^2\text{-}O)_3]$ Cores: Structures, Spectroscopy, and Core Interconversions. *J. Am. Chem. Soc.* **1999**, *121* (10), 2226-2235 DOI: 10.1021/ja983615t.

(21) Fout, A. R.; Zhao, Q.; Xiao, D. J.; Betley, T. A. Oxidative Atom-Transfer to a Trimanganese Complex To Form $Mn_6(\mu^6\text{-}E)$ (E = O, N) Clusters Featuring Interstitial Oxide and Nitride Functionalities. *J. Am. Chem. Soc.* **2011**, *133* (42), 16750-16753 DOI: 10.1021/ja2066384.

(22) Powers, T. M.; Betley, T. A. Testing the Polynuclear Hypothesis: Multielectron Reduction of Small Molecules by Triiron Reaction Sites. *J. Am. Chem. Soc.* **2013**, *135* (33), 12289-12296 DOI: 10.1021/ja405057n.

(23) Lionetti, D.; Day, M. W.; Agapie, T. Metal-templated ligand architectures for trinuclear chemistry: tricopper complexes and their O_2 reactivity. *Chem. Sci.* **2013**, *4* (2), 785-790 DOI: 10.1039/C2SC21758A.

(24) Chan, S. I.; Lu, Y.-J.; Nagababu, P.; Maji, S.; Hung, M.-C.; Lee, M. M.; Hsu, I. J.; Minh, P. D.; Lai, J. C. H.; Ng, K. Y.; et al. Efficient Oxidation of Methane to Methanol by Dioxygen Mediated by Tricopper Clusters. *Angew. Chem. Int. Ed.* **2013**, *52* (13), 3731-3735 DOI: 10.1002/anie.201209846.

(25) Herbert, D. E.; Lionetti, D.; Rittle, J.; Agapie, T. Heterometallic Triiron-Oxo/Hydroxo Clusters: Effect of Redox-Inactive Metals. *J. Am. Chem. Soc.* **2013**, *135* (51), 19075-19078 DOI: 10.1021/ja4104974.

(26) Brinkmeier, A.; Schulz, R. A.; Buchhorn, M.; Spyra, C.-J.; Dechert, S.; Demeshko, S.; Krewald, V.; Meyer, F. Structurally Characterized μ-1,2-Peroxo/Superoxo Dicopper(II) Pair. *J. Am. Chem. Soc.* **2021**, *143* (27), 10361-10366 DOI: 10.1021/jacs.1c04316.

(27) Mondal, S.; Zhang, W.; Zhang, S. Thermodynamics of Proton-Coupled Electron Transfer at Tricopper μ-Oxo/Hydroxo/Aqua Complexes. *J. Am. Chem. Soc.* **2024**, *146* (22), 15036-15044 DOI: 10.1021/jacs.3c14420.
(28) Wang, L.; Gennari, M.; Cantú Reinhard, F. G.; Padamati, S. K.; Philouze, C.; Flot, D.; Demeshko, S.; Browne, W. R.; Meyer, F.; de Visser, S. P.; et al. O_2 Activation by Non-Heme Thiolate-Based Dinuclear Fe Complexes. *Inorg. Chem.* **2020**, *59* (5), 3249-3259 DOI: 10.1021/acs.inorgchem.9b03633.
(29) Duan, P.-C.; Manz, D.-H.; Dechert, S.; Demeshko, S.; Meyer, F. Reductive O_2 Binding at a Dihydride Complex Leading to Redox Interconvertible μ -1,2-Peroxo and μ -1,2-Superoxo Dinickel(II) Intermediates. *J. Am. Chem. Soc.* **2018**, *140* (14), 4929-4939 DOI: 10.1021/jacs.8b01468.
(30) Winslow, C.; Lee, H. B.; Field, M. J.; Teat, S. J.; Rittle, J. Structure and Reactivity of a High-Spin, Nonheme Iron(III)-Superoxo Complex Supported by Phosphinimide Ligands. *J. Am. Chem. Soc.* **2021**, *143* (34), 13686-13693 DOI: 10.1021/jacs.1c05276.
(31) Dehnicke, K.; Krieger, M.; Massa, W. Phosphoraneiminato complexes of transition metals. *Coord. Chem. Rev.* **1999**, *182* (1), 19-65 DOI: 10.1016/S0010-8545(98)00191-X.
(32) Aguirre Quintana, L. M.; Yang, Y.; Ramanathan, A.; Jiang, N.; Bacsa, J.; Maron, L.; La Pierre, H. S. Chalcogen-atom abstraction reactions of a Di-iron imidophosphorane complex. *Chem. Commun.* **2021**, *57* (54), 6664-6667 DOI: 10.1039/d1cc02195h.
(33) Rice, N. T.; McCabe, K.; Bacsa, J.; Maron, L.; La Pierre, H. S. Two-Electron Oxidative Atom Transfer at a Homoleptic, Tetravalent Uranium Complex. *J. Am. Chem. Soc.* **2020**, *142* (16), 7368-7373 DOI: 10.1021/jacs.0c02693.
(34) Winslow, C. C.; Rathke, P.; Rittle, J. Multielectron Bond Cleavage Processes Enabled by Redox-Responsive Phosphinimide Ligands. *Inorg. Chem.* **2023**, *62* (43), 17697-17704 DOI: 10.1021/acs.inorgchem.3c02307.
(35) Aguirre Quintana, L. M.; Rajeshkumar, T.; Jiang, N.; Niklas, J. E.; Bacsa, J.; Maron, L.; La Pierre, H. S. Elemental chalcogen reactions of a tetravalent uranium imidophosphorane complex: cleavage of dioxygen. *Chem. Commun.* **2022**, *58* (95), 13242-13245 DOI: 10.1039/D2CC05066H.
(36) Niklas, J. E.; Studvick, C. M.; Bacsa, J.; Popov, I. A.; La Pierre, H. S. Ligand Control of Oxidation and Crystallographic Disorder in the Isolation of Hexavalent Uranium Mono-Oxo Complexes. *Inorg. Chem.* **2023**, *62* (5), 2304-2316 DOI: 10.1021/acs.inorgchem.2c04056.
(37) Lee, H. B.; Ciolkowski, N.; Winslow, C.; Rittle, J. High Spin Cobalt Complexes Supported by a Trigonal Tris(Phosphinimide) Ligand. *Inorg. Chem.* **2021**, *60* (16), 11830-11837 DOI: 10.1021/acs.inorgchem.1c01400.
(38) Hernández Sánchez, R.; Bartholomew, A. K.; Powers, T. M.; Ménard, G.; Betley, T. A. Maximizing Electron Exchange in a $[Fe_3]$ Cluster. *J. Am. Chem. Soc.* **2016**, *138* (7), 2235-2243 DOI: 10.1021/jacs.5b12181.
(39) Pandelia, M.-E.; Lanz, N. D.; Booker, S. J.; Krebs, C. Mössbauer spectroscopy of Fe/S proteins. *Biochim. et Biophys. Acta (BBA) - Mol. Cell Res.* **2015**, *1853* (6), 1395-1405 DOI: 10.1016/j.bbamcr.2014.12.005.
(40) MacDonnell, F. M.; Ruhlandt-Senge, K.; Ellison, J. J.; Holm, R. H.; Power, P. P. Sterically Encumbered Iron(II) Thiolate Complexes: Synthesis and Structure of Trigonal Planar $[Fe(SR)_3]^-$ (R = 2,4,6-t-$Bu_3C_6H_2$) and Moessbauer Spectra of Two- and Three-Coordinate Complexes. *Inorg. Chem.* **1995**, *34* (7), 1815-1822 DOI: 10.1021/ic00111a032.
(41) Lee, H. B.; Shiau, A. A.; Marchiori, D. A.; Oyala, P. H.; Yoo, B.-K.; Kaiser, J. T.; Rees, D. C.; Britt, R. D.; Agapie, T. $CaMn_3^{IV}O_4$ Cubane Models of the Oxygen-Evolving Complex: Spin Ground States S<9/2 and the Effect of Oxo Protonation. *Angew. Chem. Int. Ed.* **2021**, *60* (32), 17671-17679 DOI: 10.1002/anie.202105303.
(42) Tsui, E. Y.; Kanady, J. S.; Day, M. W.; Agapie, T. Trinuclear first row transition metal complexes of a hexapyridyl, trialkoxy 1,3,5-triarylbenzene ligand. *Chem. Commun.* **2011**, *47* (14), 4189-4191 DOI: 10.1039/c0cc05608a.
(43) Lee, Y.; Anderton, K. J.; Sloane, F. T.; Ermert, D. M.; Abboud, K. A.; García-Serres, R.; Murray, L. J. Reactivity of Hydride Bridges in High-Spin [3M-3(μ-H)] Clusters (M = Fe^{II}, Co^{II}). *J. Am. Chem. Soc.* **2015**, *137* (33), 10610-10617 DOI: 10.1021/jacs.5b05204.
(44) Kahn, O. Dinuclear Complexes with Predictable Magnetic Properties. *Angew. Chem. Int. Ed. in English* **1985**, *24* (10), 834-850 DOI: 10.1002/anie.198508341.
(45) Chakarawet, K.; Atanasov, M.; Marbey, J.; Bunting, P. C.; Neese, F.; Hill, S.; Long, J. R. Strong Electronic and Magnetic Coupling in M_4 (M = Ni, Cu) Clusters via Direct Orbital Interactions between Low-Coordinate Metal Centers. *J. Am. Chem. Soc.* **2020**, *142* (45), 19161-19169 DOI: 10.1021/jacs.0c08460.
(46) Yang, L.; Powell, D. R.; Houser, R. P. Structural variation in copper(i) complexes with pyridylmethylamide ligands: Structural analysis with a new four-coordinate geometry index, τ4. *J. Chem. Soc. Dalton Trans.* **2007**, (9), 955-964 DOI: 10.1039/b617136b.
(47) Sato, T.; Ambe, F.; Endo, K.; Katada, M.; Maeda, H.; Nakamoto, T.; Sano, H. Mixed-Valence States of $[Fe_3O(CH_2XCO_2)_6(H_2O)_3]\cdot nH_2O$ (X = H, Cl, and Br) Characterized by X-ray Crystallography and ^{57}Fe-Mössbauer Spectroscopy. *J. Am. Chem. Soc.* **1996**, *118* (14), 3450-3458 DOI: 10.1021/ja953038y.
(48) Saalfrank, R. W.; Trummer, S.; Krautscheid, H.; Schünemann, V.; Trautwein, A. X.; Hien, S.; Stadler, C.; Daub, J. A Neutral, Triple-Helical, Trinuclear, Oxo-Centered Mixed-Valence Iron Complex. *Angew. Chem. Int. Ed. in English* **1996**, *35* (19), 2206-2208 DOI: 10.1002/anie.199622061.
(49) Nakamoto, T.; Hanaya, M.; Katada, M.; Endo, K.; Kitagawa, S.; Sano, H. The Valence-Detrapping Phase Transition in a Crystal of the Mixed-Valence Trinuclear Iron Cyanoacetate Complex $[Fe_3O(O_2CCH_2CN)_6(H_2O)_3]$. *Inorg. Chem.* **1997**, *36* (20), 4347-4359 DOI: 10.1021/ic961438w.
(50) Coropceanu, V.; Schünemann, V.; Ober, C.; Gerdan, M.; Trautwein, A. X.; Köhler, J.; Saalfrank, R. W. A neutral triple-helical trinuclear oxo-centered mixed-valent iron complex: Mossbauer spectroscopic and magnetic susceptibility studies. *Inorg. Chim. Acta* **2000**, *300-302*, 875-881 DOI: 10.1016/S0020-1693(00)00003-7.
(51) Wu, R.; Poyraz, M.; Sowrey, F. E.; Anson, C. E.; Wocadlo, S.; Powell, A. K.; Jayasooriya, U. A.; Cannon, R. D.; Nakamoto, T.; Katada, M.; et al. Electron Localization and Delocalization in Mixed-Valence Transition Metal Clusters: Structural and Spectroscopic Studies of Oxo-Centered Trinuclear Complexes $[Fe_3O(OOCCMe_3)_6(py)_3]^{+/0}$ and $[Mn_3O(OOCCMe_3)_6(py)_3]^{+/0}$. *Inorg. Chem.* **1998**, *37* (8), 1913-1921 DOI: 10.1021/ic970451t.
(52) Zhang, K. L.; Shi, Y. J.; You, X. Z.; Yu, K. B. Preparation, crystal structure and characterization of a novel iron(III) oxide cluster containing two different discrete $[Fe_3O]$ units. *J. Mol. Struct.* **2005**, *743* (1-3), 73-77 DOI: 10.1016/j.molstruc.2005.02.030.
(53) Weihe, H.; Güdel, H. U. Angular and distance dependence of the magnetic properties of oxo-bridged iron(III) dimers. *J. Am. Chem. Soc.* **1997**, *119* (28), 6539-6543 DOI: 10.1021/ja970320r.
(54) Zhao, Q.; Betley, T. A. Synthesis and redox properties of triiron complexes featuring strong Fe-Fe interactions. *Angew. Chem. Int. Ed.* **2011**, *50* (3), 709-712 DOI: 10.1002/anie.201005198.
(55) Leiszner, S. S.; Chakarawet, K.; Long, J. R.; Nishibori, E.; Sugimoto, K.; Platts, J. A.; Overgaard, J. Electron Density Analysis of Metal-Metal Bonding in a Ni_4 Cluster Featuring Ferromagnetic Exchange. *Inorg. Chem.* **2023**, *62* (1), 192-200 DOI: 10.1021/acs.inorgchem.2c03170.
(56) Chambers, M. B.; Groysman, S.; Villagrán, D.; Nocera, D. G. Iron in a Trigonal Tris(alkoxide) Ligand Environment. *Inorg. Chem.* **2013**, *52* (6), 3159-3169 DOI: 10.1021/ic302634q.
(57) Mukherjee, J.; Lucas, R. L.; Zart, M. K.; Powell, D. R.; Day, V. W.; Borovik, A. S. Synthesis, structure, and physical properties for a series of monomeric iron(III) hydroxo complexes with varying hydrogen-bond networks. *Inorg. Chem.* **2008**, *47* (13), 5780-5786 DOI: 10.1021/ic800048e.
(58) Creutz, S. E.; Peters, J. C. Spin-State Tuning at Pseudo-tetrahedral d^6 Ions: Spin Crossover in $[BP_3]Fe^{II}$-X Complexes. *Inorg. Chem.* **2016**, *55* (8), 3894-3906 DOI: 10.1021/acs.inorgchem.6b00066.
(59) Jackson, T. A.; Rohde, J.-U.; Seo, M. S.; Sastri, C. V.; DeHont, R.; Stubna, A.; Ohta, T.; Kitagawa, T.; Münck, E.; Nam, W.; et al. Axial Ligand Effects on the Geometric and Electronic Structures of Nonheme Oxoiron(IV) Complexes. *J. Am. Chem. Soc.* **2008**, *130* (37), 12394-12407 DOI: 10.1021/ja8022576.
(60) MacBeth, C. E.; Gupta, R.; Mitchell-Koch, K. R.; Young, V. G., Jr.; Lushington, G. H.; Thompson, W. H.; Hendrich, M. P.; Borovik, A. S. Utilization of Hydrogen Bonds To Stabilize M−O(H) Units: Synthesis and Properties of Monomeric Iron and Manganese Complexes with Terminal Oxo and Hydroxo Ligands. *J. Am. Chem. Soc.* **2004**, *126* (8), 2556-2567 DOI: 10.1021/ja0305151.
(61) Havlin, R. H.; Godbout, N.; Salzmann, R.; Wojdelski, M.; Arnold, W.; Schulz, C. E.; Oldfield, E. An experimental and density functional theoretical investigation of iron-57 Mossbauer quadrupole splittings in organometallic and heme-model compounds: Applications to carbonmonoxy-heme protein structure. *J. Am. Chem. Soc.* **1998**, *120* (13), 3144-3151 DOI: 10.1021/ja972619f.
(62) Proshlyakov, D. A.; Henshaw, T. F.; Monterosso, G. R.; Ryle, M. J.; Hausinger, R. P. Direct Detection of Oxygen Intermediates in the Non-

Heme Fe Enzyme Taurine/α-Ketoglutarate Dioxygenase. *J. Am. Chem. Soc.* **2004**, *126* (4), 1022-1023 DOI: 10.1021/ja039113j.
(63) Santra, G.; Neese, F.; Pantazis, D. A. Extensive reference set and refined computational protocol for calculations of ^{57}Fe Mössbauer parameters. *Phys. Chem. Chem. Phys.* **2024**, 23322-23334 DOI: 10.1039/d4cp00431k.
(64) Scepaniak, J. J.; Harris, T. D.; Vogel, C. S.; Sutter, J.; Meyer, K.; Smith, J. M. Spin crossover in a four-coordinate iron(II) complex. *J. Am. Chem. Soc.* **2011**, *133* (11), 3824-3827 DOI: 10.1021/ja2003473.
(65) Zhang, X.; Furutachi, H.; Fujinami, S.; Nagatomo, S.; Maeda, Y.; Watanabe, Y.; Kitagawa, T.; Suzuki, M. Structural and Spectroscopic Characterization of (μ -Hydroxo or μ -Oxo)(μ -peroxo)diiron(III) Complexes: Models for Peroxo Intermediates of Non-Heme Diiron Proteins. *J. Am. Chem. Soc.* **2005**, *127* (3), 826-827 DOI: 10.1021/ja045594a.
(66) Gordon, J. B.; Vilbert, A. C.; DiMucci, I. M.; MacMillan, S. N.; Lancaster, K. M.; Moënne-Loccoz, P.; Goldberg, D. P. Activation of Dioxygen by a Mononuclear Nonheme Iron Complex: Sequential Peroxo, Oxo, and Hydroxo Intermediates. *J. Am. Chem. Soc.* **2019**, *141* (44), 17533-17547 DOI: 10.1021/jacs.9b05274.
(67) Costas, M.; Rohde, J.-U.; Stubna, A.; Ho, R. Y. N.; Quaroni, L.; Münck, E.; Que, L. A Synthetic Model for the Putative $Fe^{IV2}O_2$ Diamond Core of Methane Monooxygenase Intermediate Q. *J. Am. Chem. Soc.* **2001**, *123* (51), 12931-12932 DOI: 10.1021/ja017204f.
(68) Alborés, P.; Rentschler, E. A T-Shaped μ^3-Oxido Trinuclear Iron Cluster with High Easy-Plane Anisotropy: Structural and Magnetic Characterization. *Eur. J. Inorg. Chem.* **2008**, *2008* (25), 4004-4011 DOI: 10.1002/ejic.200800327.
(69) Girerd, J. J.; Papaefthymiou, G. C.; Watson, A. D.; Gamp, E.; Hagen, K. S.; Edelstein, N.; Frankel, R. B.; Holm, R. H. Electronic properties of the linear antiferromagnetically coupled clusters $[Fe_3S_4(SR)_4]^{3-}$, structural isomers of the iron-sulfur(1+) ($[Fe_3S_4]^{1+}$) unit in iron-sulfur proteins. *J. Am. Chem. Soc.* **1984**, *106* (20), 5941-5947 DOI: 10.1021/ja00332a031.
(70) Boudalis, A. K.; Sanakis, Y.; Raptopoulou, C. P.; Terzis, A.; Tuchagues, J.-P.; Perlepes, S. P. A trinuclear cluster containing the $\{Fe_3(\mu^3\text{-}O)\}^{7+}$ core: Structural, magnetic and spectroscopic (IR, Mössbauer, EPR) studies. *Polyhedron* **2005**, *24* (12), 1540-1548 DOI: 10.1016/j.poly.2005.04.016.
(71) Ali, G.; VanNatta, P. E.; Ramirez, D. A.; Light, K. M.; Kieber-Emmons, M. T. Thermodynamics of a μ-oxo Dicopper(II) Complex for Hydrogen Atom Abstraction. *J. Am. Chem. Soc.* **2017**, *139* (51), 18448-18451 DOI: 10.1021/jacs.7b10833.
(72) Warm, K.; Paskin, A.; Kuhlmann, U.; Bill, E.; Swart, M.; Haumann, M.; Dau, H.; Hildebrandt, P.; Ray, K. A Pseudotetrahedral Terminal Oxoiron(IV) Complex: Mechanistic Promiscuity in C−H Bond Oxidation Reactions. *Angew. Chem. Int. Ed.* **2021**, *60* (12), 6752-6756 DOI: 10.1002/anie.202015896.
(73) Que, J. L.; Tolman, W. B. Bis(μ-oxo)dimetal "Diamond" Cores in Copper and Iron Complexes Relevant to Biocatalysis. *Angew. Chem. Int. Ed.* **2002**, *41* (7), 1114-1137 DOI: 10.1002/1521-3773(20020402)41:7<1114::AID-ANIE1114>3.0.CO;2-6.

TOC Graphic